Equatorial Rossby waves on Cold Surge Days and their impact on rainfall

Received: 31 October 2022 | Revised: 22 March 2023 | Accepted: 15 May 2023

DOI: 10.1002/qj.4493

Quarterly Journal of the Royal Meteorological Society RMetS

RESEARCH ARTICLE

Equatorial Rossby waves on cold surge days and their impact on rainfall

Jeong-Yik Diong[1] | **Prince Xavier**[2] | **Steven J. Woolnough**[3] | **Firdaus Ammar Abdullah**[1]

[1]Research and Technical Development Division, Malaysia Meteorological Department, Petaling Jaya, Malaysia

[2]Met Office, Exeter, UK

[3]National Centre of Atmospheric Science, Department of Meteorology, University of Reading, Reading, UK

Correspondence
Jeong-Yik Diong, Research and Technical Development Division, Malaysia Meteorological Department, Petaling Jaya, Selangor, Malaysia.
Email: diong@met.gov.my

Funding information
NCAS ODA national capability program ACREW, Grant/Award Number: NE/R000034/1; Newton-Ungku Omar Fund; Weather and Climate Science for Services Partnership; National Centre for Atmospheric Science; Met Office Weather and Science for Services Partnership

Abstract

This study aims to understand the process that determines the regional rainfall distribution in the equatorial South China Sea (SCS) and its surrounding during the cold surge (CS) days by looking at the different vorticity phases of active equatorial Rossby (R1) waves and the dynamics of the CSs related to the R1 wave. The CS can be thought of as an anticyclonic outflow from midlatitude and behaves like a dispersive group of R1 meridional modes. From the study, it shows the vorticity of the R1 wave arranges itself in such a way that the anticyclonic phase is located to the west and the cyclonic phase is located to the east of the cold CS axis. The CS winds in the equatorial SCS occur early, remain longer, and possess a larger zonal component in the active cyclonic phase compared with the active anticyclonic phase. During the active cyclonic vorticity phase, the rainfall anomalies pattern in the equatorial SCS changes from a "tick-mark-like" pattern to a "V-shape" pattern as a consequence of the westward propagation of the wave. The probability of rainfall increases near the centre of cyclonic vorticity, but for anticyclonic vorticity the probability increases in the southern part of the vorticity centre. There is both increased (decreased) intensity and probability of extreme rainfall events during the active cyclonic (anticyclonic) vorticity phase on CS days. Overall, the rainfall anomalies are largely dominated by changes in the intensity on wet days rather than the number of wet days. These changes indicate the roles of the R1 wave vorticity phase in the rainfall distribution during CS days. The timing of enhancement and suppression of rain will provide additional valuable information to help improve forecast extreme weather events.

KEYWORDS

cold surge, equatorial Rossby wave, South China Sea

1 | INTRODUCTION

The outbreak of very cold air from midlatitudes to the Equator is one of the dramatic weather events in the Maritime Continent (MC) during the Asian winter monsoon. The equatorward surge of cold air is predominantly a lower tropospheric phenomenon, and the acceleration of northeasterly winds is generally confined below 700 hPa and is associated with the southward intrusions of the Siberian–Mongolian high. It often causes sustained convection over the MC (Ramage, 1971; Wu and Chan, 1995; Chang *et al.*, 2006). As this cold air surges equatorward to the vicinity of the South China Sea (SCS), it is commonly known as the "cold surge" (CS) by most of the operational forecasters in the surrounding region. This cold, dry air from midlatitudes moistens over the SCS (Johnson and Houze, 1987); coupled with low-level convergence, this results in the flaring of convection in the SCS region. The CS may also interact with the existing disturbances in the equatorial region, such as vortices propagating westward from the western Pacific (Cheang, 1977; Chang *et al.*, 1979; Chen *et al.*, 2013) and the eastward-propagating Madden–Julian oscillation (MJO) (Chang *et al.*, 2005; Lim *et al.*, 2017; Xavier *et al.*, 2020). The CS typically lasts from 2 days to up to a week, often leading to extreme rainfall events and floods (Johnson and Chang, 2007; Tangang *et al.*, 2008; Pullen *et al.*, 2015; Hai *et al.*, 2017). In the SCS region, the rainfall is concentrated mainly over the windward side of the islands and peninsula, indicating the roles played by the local terrain.

The equatorial waves play an important role in modulating tropical weather. Studies show a considerable variance of tropical convection is found to be controlled by convectively coupled equatorial waves (Roundy and Frank, 2004; Kiladis *et al.*, 2009). In the MC, for instance, the convectively coupled Kelvin waves in the lower level of the troposphere have an important impact on rainfall variability in the MC (Chen *et al.*, 2019). Ferrett *et al.* (2020) show various extreme rainfall events in southeast Asia are linked to various modes of the equatorial wave. In their study, one of the factors leading to the increase in the probability of extreme rainfall events is the high-amplitude $n = 1$ Rossby (R1) wave activity that intensifies the rainfall. Similarly, Tsai *et al.* (2020) find that, during the winter monsoon period, the equatorial Rossby (ER) waves show strong positive modulation on peak rainfall intensity in the SCS–MC region. In another study, the convectively coupled ER waves double the chance of floods and increase the probability of extreme rainfall by 15–45% (Latos *et al.*, 2021; Lubis and Respati, 2021). The convection of the ER waves is often associated with their low-level convergence (Liebmann and Hendon, 1990; Wheeler and Kiladis, 1999; Wheeler *et al.*, 2000; Yang *et al.*, 2007).

Both ER waves and CSs are known to influence the rainfall in the MC region. The rainfall linked to CSs in the southeast Asia region is due to wind–terrain interaction, whereas rainfall associated with ER waves is due to convergence or the vorticity of the wave. Lim and Chang (1981) show that the CS can be interpreted as linear wave responses to midlatitude pressure forcings by using a simple shallow-water equation. In their study, they showed that Rossby, mixed Rossby–gravity and inertia–gravity, and Kelvin modes appear in the Tropics as part of the response to the midlatitude forcing. The features of the typical CS flow pattern can be observed in the Rossby mode of response. The northeasterly CS in the equatorial region arises when the midlatitude-forcing-induced Rossby waves move at different group speeds for different meridional modes and cause the northeast–southwest tilt. The initial gravity-wave type of motion develops into a Rossby type of motion under the geostrophic adjustment on the beta plane. The fast-moving westward lower Hermite mode near the Equator and slow-moving higher Hermite mode in the midlatitudes contribute to the northeast–southwest tilt and strong northeasterly wind. Hence, the gravity-wave type of motions in the initial stage of the cold air outburst, which is mainly northerly, turn northeasterly. Although the theory successfully shows that the monsoon surge is the result of the Rossby wave response, to the best of the our knowledge, there have been almost no detailed observational studies carried out to confirm the predictions of the dynamical theory. In this study, we intend to verify the theory put forth by Lim and Chang (1981) with the observational ER waves produced using the European Centre for Medium-Range Weather Forecasts Reanalysis (ERA)-Interim (INT) dataset and explore the impact on the rainfall distribution in the MC region during CS days in different vorticity phases of active ER waves.

This paper is organized as follows. Section 2 describes the data and methods, including the definitions of the CS and the wave activity analysis. Section 3 describes the climatology of the CS and R1 wave in November–March (NDJFM). Section 4 explores the CS days that coincide with the cyclonic and anticyclonic vorticity phase of active R1 waves, the extreme rainfall distribution in MC during CS days on active R1 wave days, and some dynamics related to each different vorticity phase. Concluding remarks are provided in Section 5.

2 | DATA AND METHODS

This study covers 20 seasons of NDJFM for the period spanning 1998–2018. The months November and March are included in this study on the basis that CS events can

TABLE 1 Cold surge (CS) frequency

Cold surge	November	December	January	February	March	November–March
Total days of CS	29 (1.0%)	172 (5.7%)	237 (7.8%)	145 (4.8%)	56 (1.9%)	639 (21.1%)
Average CS days per season	1.4	8.6	11.9	7.3	2.8	32

Note: Percentages are calculated with respect to the total number of days in the 20 November–March seasons.

be observed as early as November and as late as March. Daily mean-sea-level pressure (MSLP) and low-level wind at 850 hPa are obtained from ERA-INT at 1×1 and 0.75×0.75 resolutions respectively (Dee *et al.*, 2011). Daily mean precipitation data are obtained from the TRMM 3B42 v7 dataset with a resolution of $0.25 \times 0.25°$ (Huffman *et al.*, 2007).

The CS events used in this study are identified using the definition from Lim *et al.* (2017). The CS day is defined when northeasterly wind averaged over the SCS (5°–10°N, 107°–115°E) at 850 hPa exceeds a threshold equalling 0.75 times the standard deviation above the long-term mean (northeasterly windspeed exceeding 9.07 $m \cdot s^{-1}$) and averaged MSLP over (105–122°E, 18–22°N) exceeding 1,020 hPa for at least two consecutive days or if there is a break in northeasterly wind speed (when the northeasterly winds speed fall back to less than 9.07 $m \cdot s^{-1}$) of not more than two consecutive days. The temporal criteria are given as such because CSs are often observed continuously over some time with few brief pauses. The use of MSLP is to ensure that the CSs are associated with the strong northeasterly winds from midlatitudes and thus eliminate the possibility of strong winds from tropical disturbances being flagged as CS events. Statistics of the identified CSs are shown in Table 1.

The equatorial wave used in this study is produced by the University of Reading under the funding of the Weather and Climate Science for Services Partnership for Southeast Asia project, as described in Ferrett *et al.* (2020). The zonal wind, meridional wind, and geopotential height from ERA-INT are used to produce the equatorial dataset using the method prescribed by Yang *et al.* (2003). In this method, the equatorial waves are identified by projecting the dynamical fields in the Tropics at each pressure level onto a set of horizontal structure basic functions described by parabolic cylinder functions in the meridional direction and sinusoidal variation in the zonal direction. The projection onto the waves is done independently at each pressure level and the theoretical dispersion relationship is not assumed. By doing so, this approach can account for the Doppler shifting caused by the background winds. This is particularly important, as both the mixed Rossby–gravity and Rossby waves are sensitive to the change in the background flow. The wave data are derived by the dynamical field only and have no prior information of precipitation. The dataset consists of 10 pressure levels with a spatial resolution of 1×1 and a 6 hr temporal resolution covering the 24°S–24°N latitudinal belt. The waves produced have zonal wave numbers k ranging from 2 to 40, and a period of 2–30 days covers from 1997 to 2018. Owing to the availability of satellite-derived precipitation data, the ER wave used in this study covers the period from 1998 to 2018, which accounts for 20 NDJFM seasons. The gravest meridional mode of ER waves will be used and hereafter will be known as the R1 wave.

The vorticity for the R1 wave is chosen to describe the wave amplitude since the wave is dominated by its rotational flow. Furthermore, cyclonic and anticyclonic circulation is also discussed in the theoretical work of Lim and Chang (1981). Therefore, the vorticity of the R1 wave at 850 hPa is taken for NDJFM of 1998–2018 in this study. Because the meridional structure of the waves is defined by the parabolic cylinder functions, we can use any latitude (except the node at the Equator) to define the local amplitude of the wave field. We choose to use a latitude of 8°N, as this is close to the maximum of the meridional velocity for the R1 wave. Days with the R1 vorticity at a given longitude that exceed 1.0 standard deviation from all R1 wave vorticity at that longitude from 1998 through 2018 are flagged as active wave days. Active wave days with positive and negative vorticity in the selected longitude will be known respectively as active cyclonic and anticyclonic vorticity phases. Wave activity at longitude ranges 100°–105°E, 105°–110°E, and 110°–115°E is considered for analysis. The statistics of the R1 wave vorticity phases in the three different separate longitudinal bands are provided in Table 2, which also provides statistics on the co-occurrence of active R1 wave days and CS days.

3 | CLIMATOLOGY OF THE CS, AND ACTIVE R1 WAVE

Table 1 shows that about 21% of the total 3,020 days in 20 boreal winter seasons are identified as CS days. The composite of CS events shows that high rainfall intensity centres are generally observed on the windward side of the terrain, namely over the southeastern Philippines, north of Borneo, and southeastern Peninsular Malaysia (Figure 1).

TABLE 2 Frequency of $n = 1$ Rossby (R1) wave and active R1 wave in 20 November–March (NDJFM) seasons

	Number of days		Number of active wave days	
Longitudinal band	**Cyclonic**	**Anticyclonic**	**Cyclonic**	**Anticyclonic**
100°–105°E	1,511	1,509	454 (15%)	445 (15%)
	243 (38%)	*396 (62%)*	*54 (9%)*	*134 (21%)*
105°–110°E	1,458	1,562	465 (15%)	455 (15%)
	248 (39%)	*391 (61%)*	*59 (9%)*	*135 (21%)*
110°–115°E	1,453	1,567	442 (15%)	448 (15%)
	300 (47%)	*339 (53%)*	*81 (13%)*	*88 (14%)*

Note: The frequencies of the R1 wave and active R1 wave on cold surge days are also given (in italics). Percentages in the parentheses, except on cold surge days (in italics) are calculated with respect to the total number of days in 20 NDJFM seasons. The percentages during cold surge days are calculated with respect to the total number of cold surge days in the 20 NDJFM seasons.

This results from the interaction between the CS winds blowing perpendicular to the coast and the complex local terrains found on the islands and peninsula in the MC. In the SCS, the CS northeasterly winds converge with broad easterly winds from the western Pacific. Rainfall is also observed on the northwestern coast of Borneo. The northeasterly winds parallel to the Borneo coastline provide copious shear vorticity in this region, and thus the concentration of rainfall in this region (Chang *et al.*, 2005a). On occasions, the shear and curvature vorticity in Borneo can intensify into a vortex and is known as the Borneo vortex, and this may interact with the CS and may produce heavy rainfall events (Chang *et al.*, 2003; Tangang *et al.*, 2008). These northeasterly winds that are parallel along the Borneo coastline will then turn anticlockwise when they cross the Equator and become westerly winds due to the conservation of potential vorticity. These westerly winds bring heavy rains to the Indonesian monsoon region.

During CS days, the composite R1 wave is organized with anticyclonic vorticity located to the west and cyclonic vorticity located to the east of 115°E, as shown in Figure 1. This suggests that the CS main axis in the SCS is located to the east of 115°E. The Kolmogorov–Smirnov test reveals the distribution of the vorticity phases on CS days is significantly different at the 0.05 significance level from all NDJFM days. Although R1 is the gravest mode, such vorticity phase arrangement and northeasterly winds that give rise to the northeast–southwest tilt in the surge axis are consistent with the meridional dispersion of a group of ER waves with different meridional wave numbers under surge condition proposed by Lim and Chang (1981). The anomalous fields show that, during CS events, the excess rainfall band is located near the Equator while the deficit rainfall band is located above 10°N (Figure 1b). These form the wet and dry anomalies northeast–southwest tilt parallel dipole. The dipole can be thought to arise from the southward transport of moisture by the freshening northeasterlies. While in the north, the advection of colder sea-surface temperature from midlatitude into the northern SCS by the CS suppresses deep convection in the region. This northeast–southwest tilt parallel dipole also corresponds to the differential westward movement of Rossby wave modes. The rainfall and its anomalies have a distinct "tick-mark-like" pattern in the SCS region, as noted in a previous study (Lim *et al.*, 2017), with a long northeast–southwest band of enhanced rainfall off the coast of Borneo and a short northwest–southeast titled band of rainfall off the coast of Peninsular Malaysia.

Figure 2a,b shows composites of the anomalies of active wave day precipitation from the NDJFM seasonal mean. Of the total 3,020 days in the 20 boreal winter seasons, about 30% of the total days are identified as active wave days (Table 2). This is roughly consistent with the wave amplitude being normally distributed. The rainfall anomalies on R1 active wave days are located in the region where the wave is active, with enhanced rainfall observed around the vicinity of cyclonic phases of the active R1 wave and suppressed rainfall found elsewhere. However, it should also be noted that the strong cyclonic vorticity (and hence the active wave day) and the rainfall increases could be contributed by tropical cyclones in the wave identification region, as shown by Ferrett *et al.*, (2020). During the anticyclonic phases of the active R1 wave, the rainfall anomaly distribution patterns are nearly identically opposite. Thus, dry–wet–dry and wet–dry–wet patterns are discernible in the cyclonic and anticyclonic phase composites respectively. It is observed that the rainfall anomalies weaken when the R1 wave propagates westward from the SCS into the Peninsular Malaysia and Sumatra region. In addition to that, rainfall anomaly signals are generally larger in the Northern Hemisphere than in the Southern Hemisphere when the active vorticity phases are located

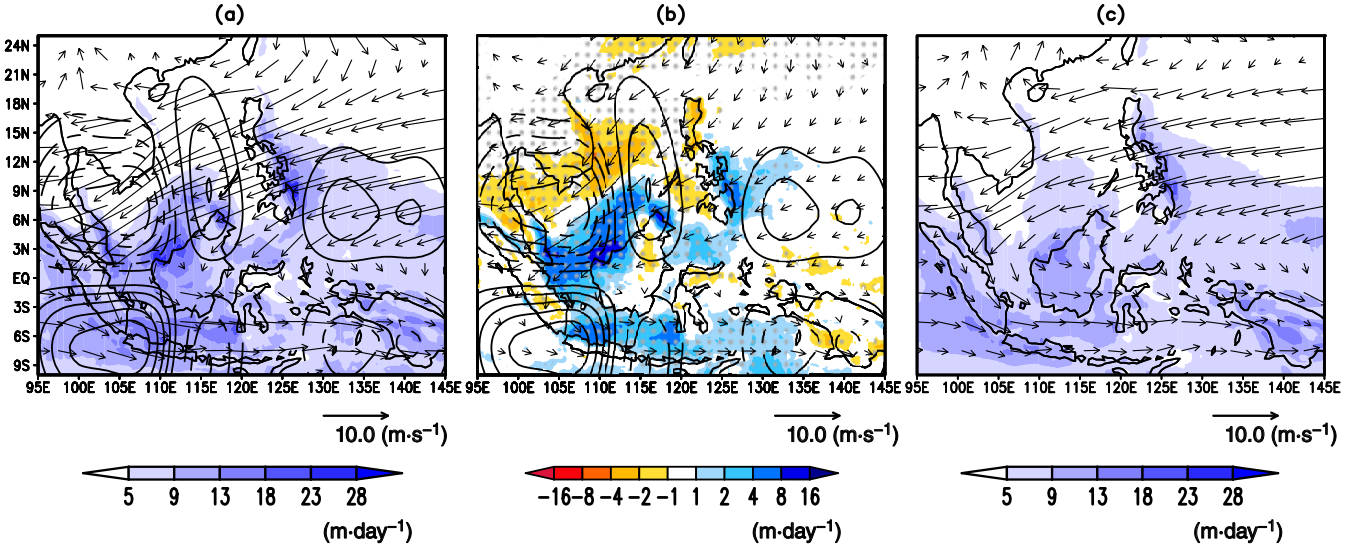

FIGURE 1 (a) Composites mean for rainfall, wind, and $n = 1$ Rossby (R1) wave vorticity on a cold surge (CS) day for 20 November–March (NDJFM) seasons (1998–2017); (b) CS day composite anomaly for the rainfall and wind (minus NDJFM mean) and the R1 wave vorticity; (c) NDJFM seasonal mean of 1998–2017. Rainfall (shaded contour); R1 wave vorticity (contours starting $\pm 2 \times 10^{-6}$ s^{-1} with an interval of 2×10^{-6} s^{-1}), 850 hPa wind (vector). Stippling indicates regions where composite rainfall is significantly different from the 1998 to 2017 NDJFM seasonal mean at the 95% confidence level based on Student's *t*-test [Colour figure can be viewed at wileyonlinelibrary.com]

to the east of 100°–105°E. However, when there are active vorticity phases in 100°–105°E, large anomalies shifted to the Southern Hemisphere. This could be due to the modification of rainfall signals by the terrains and also, much more likely, due to the association with tropical cyclones in the Northern Hemisphere. Along with the anomalous rainfall concentrated around the vorticity, anomalous rainfall also corresponds to the zonal wind anomaly near the Equator. Enhanced (suppressed) rainfall anomalies are found in the anomalous easterlies (westerlies) near the equatorial belt, suggesting the role of the surface flux convergence played by the R1 wave. In the SCS, winds are anomalously southwesterly when the active R1 wave is in the cyclonic vorticity phase and anomalously northeasterly when the R1 wave is in the anticyclonic phase. These anomalous winds during the active wave days resemble the theoretical wave structure. Thus, the wind circulation during the R1 wave cyclonic vorticity phase is anomalously opposite to the background monsoonal flow. The opposite effect is also seen off the west coast of Java, where the wind anomalies are enhancing the climatological westerly in the Australian monsoon.

The effect of CS on the active R1 waves in each longitudinal band is shown in Figure 2c,d, by considering only active wave days without a CS. The impact of the CS on the wave composite is small for the cyclonic phase and is entirely consistent with the fact that only a small percentage of the active cyclonic phase coincides with a CS. One of the largest differences is found in the anticyclonic phase, suggesting the largest effect of the CS when the CS coincides with the active anticyclonic phase. Figure 2d suggests that the anomalous rainfall around the Equator found in Figure 2b in longitudinal bands 100–105°E and 105–110°E is contributed by the effect of the CS. The anomalous winds in the Northern Hemisphere are almost in the opposite direction, whereby when the CS days are removed from the composites the winds become southerlies in the SCS. This indicates that the anomalous winds during this vorticity phase minus the CS days do not resemble the theoretical wave structure. This suggests that these waves may be embedded in some other large-scale weather structures. The effect of CS days coinciding with active waves will be investigated further in Section 4.

4 | CS ON ACTIVE WAVE DAYS

4.1 | CS on active wave days climatology

During CS days, the vorticity of R1 waves in the selected longitudes is mainly anticyclonic (more than 50% of the total surge days; Table 2), although the frequency of the cyclonic and anticyclonic vorticity occurrences are almost equally the same in NDJFM. The occurrences of the active anticyclonic phase are 1.5 or 2 times higher than the active cyclonic phase in the 100°–105°E and 105°–110°E bands during CS days. However, for the 110°–115°E band, there is no preference of phase. These statistics are consistent with the composite mean of the R1 wave during CS days, as shown in Figure 1, and show the vorticity of the R1

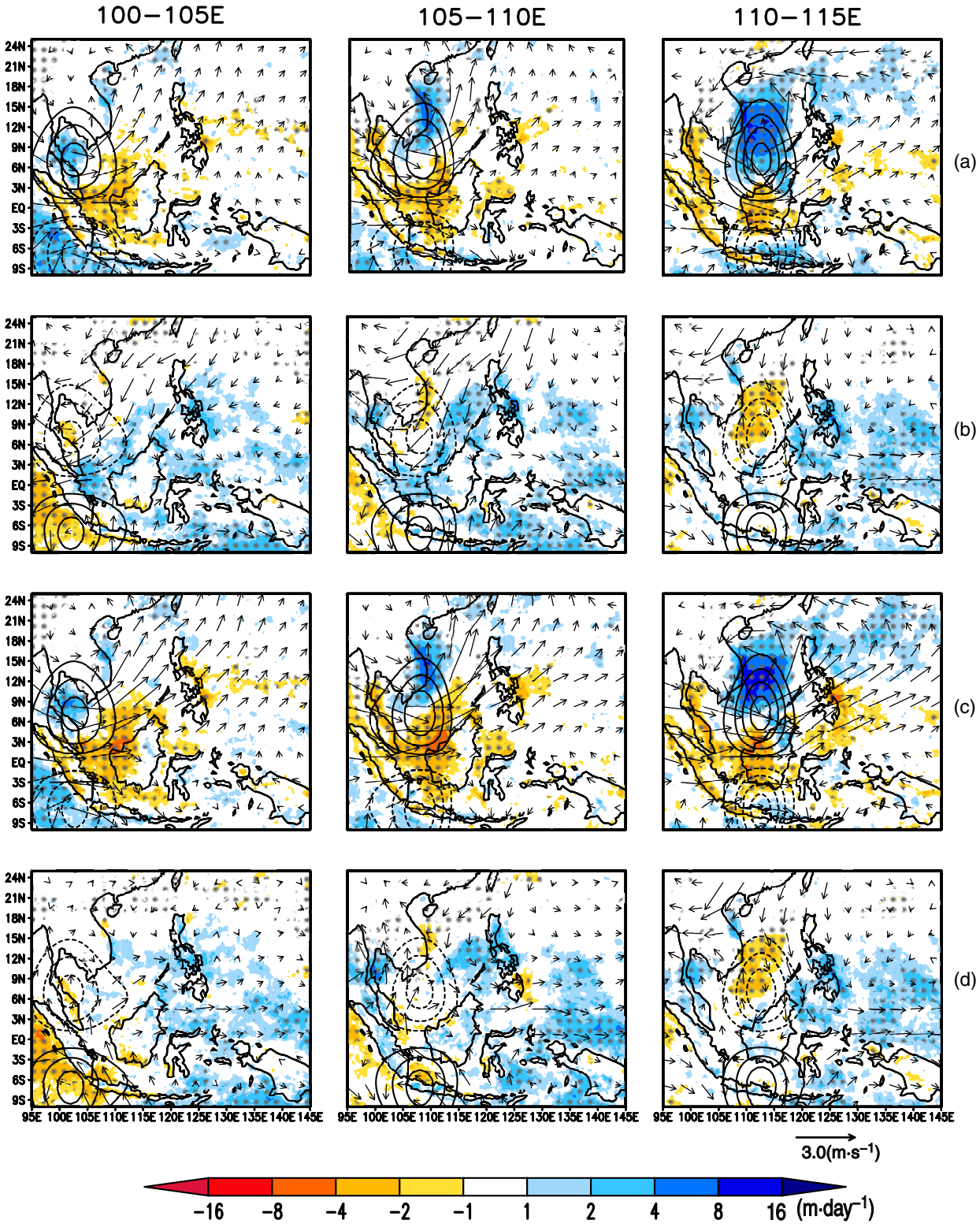

FIGURE 2 Composite anomaly of rainfall and low-level wind during active $n = 1$ Rossby (R1) wave day in the longitudinal band of 100°–105°E, 105°–110°E, and 110°–115°E for 20 November–March (NDJFM) seasons. (a) All active wave days with cyclonic vorticity phase; (b) all active wave days with anticyclonic vorticity phase; (c) active wave days with cyclonic vorticity phase without cold surge (CS); (d) active wave days with anticyclonic vorticity phase without CS. Rainfall (shaded contour), R1 vorticity (contours begin with $\pm 2 \times 10^{-5}$ s^{-1} with an interval of 2×10^{-5} s^{-1}), and 850 hPa wind(vector). The 20 NDJFM seasonal mean is removed from the data to get the anomaly. Stippling indicates regions where anomaly is significantly different from the 20 NDJFM seasonal mean at the 95% confidence level based on Student's *t*-test [Colour figure can be viewed at wileyonlinelibrary.com]

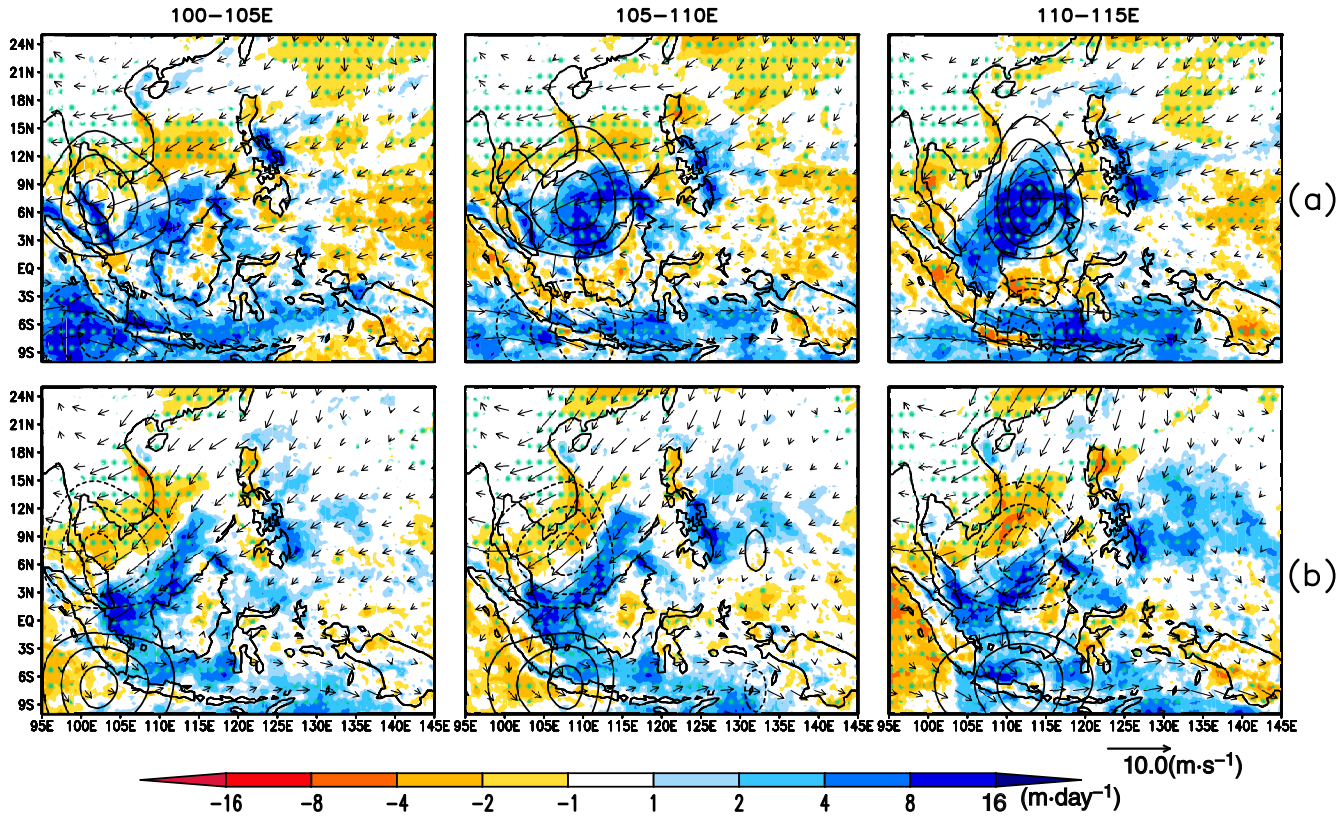

FIGURE 3 Composite anomaly of rainfall and low-level wind during active $n = 1$ Rossby wave on cold surge days in the longitudinal band of 100°–105°E, 105°–110°E, and 110°–115°E for 20 November–March (NDJFM) seasons for rainfall and low-level winds. (a) Wave days with cyclonic vorticity phase; (b) wave days with anticyclonic vorticity phase. Rainfall (shaded contour), vorticity (contour), and 850 hPa wind (vector). The 20 NDJFM seasonal mean is removed from the rainfall and wind data to get the anomaly fields. Stippling indicates regions where anomaly is significantly different from the 20 NDJFM seasonal mean at the 95% confidence level based on Student's *t*-test [Colour figure can be viewed at wileyonlinelibrary.com]

wave favours an anticyclonic vorticity phase during CS days. The statistics also suggest that, since most of the vorticity is anticyclonic when the R1 waves are identified in the longitude west of 110°–115°E, the path or the axis of the CS northeasterlies is located between the longitude of 100° and 110°E. If the CS is dynamically thought to be the meridional dispersion of the anticyclonic phase of the Rossby mode on the beta plane, the question remains as to why there are CS days with a cyclonic phase of the Rossby wave. We will explore this in Section 4.3.

Figure 3a,b shows the composite of CS days on active R1 waves with the cyclonic and anticyclonic vorticity phase in each longitudinal band. Generally, the dry–wet–dry (wet–dry–wet) anomalies found in the cyclonic (anticyclonic) vorticity phase on CS days are not discernible as all active wave days (Figure 2) due to the presence of shear vorticity and wind–terrain-induced rainfall. One obvious example is the rainfall anomalies that run parallel to the Borneo coast (induced mainly by the shear vorticity) and on the windward side along the east coast of Peninsular Malaysia and the Philippines. The suppressed rainfall anomaly regions in the active wave day only with cyclonic vorticity in the domain (see Figure 2a) are now replaced by the wind–terrain-enhanced rainfall associated with the CS flow. However, in the vicinity of the cyclonic (anticyclonic) phase of active waves, the enhanced (suppressed) rainfall anomaly is still expected.

In the composite of CS days with active cyclonic vorticity phase (Figure 3a), the suppressed rainfall region is found downstream of the active cyclonic vorticity region. As a result, when the active wave in this vorticity phase is located in the SCS region, northeastern Peninsular Malaysia remains anomalously dry until the active wave in this vorticity phase starts to propagate into this region. The north–south parallel dipole in the rainfall anomaly is still visible but is weaker, with the rainfall in the south extending northward and covering most of the equatorial SCS. Therefore, the large-scale wave dynamics act to extend the spatial coverage of the rainfall in the SCS–Borneo region. When the wave propagates into the Peninsular Malaysia region, it enhances the rainfall in northeastern Peninsular Malaysia. As a consequence, the

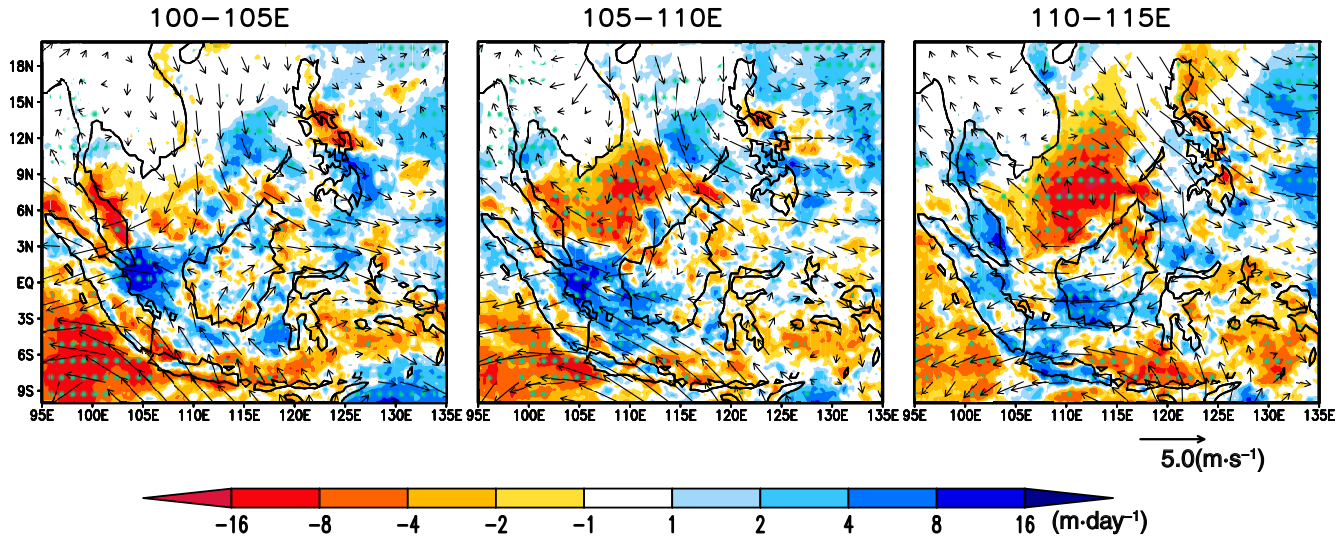

FIGURE 4 Composite difference between the anticyclonic and cyclonic phases of the $n = 1$ Rossby wave on cold surge days. Shaded (rainfall), vector (850 hPa wind). Stippling indicates regions where difference is significantly different at the 95% confidence level based on Student's *t*-test [Colour figure can be viewed at wileyonlinelibrary.com]

"tick-mark-like" pattern in the rainfall anomalies field in the equatorial SCS becomes a "V-shape" pattern, with a longer northwest–southeast-tilted rainfall band in Peninsular Malaysia. The anomalous winds in this phase do not resemble the theoretical wind structure of the wave. This indicates that the CS winds dominate those of the winds associated with the wave in this phase. The rainfall and circulation features when CSs coincide with the cyclonic vorticity phase identified in 100°–110°E (Figure 3a) are almost similar to the features during the joint occurrence of the MJO in phases 2–4 and the CS identified by Lim *et al.* (2017, fig. 6c). This indicates that the active cyclonic phase on CS days may have almost the same characteristics of joint occurrence of a CS and MJO in phases 2–4 (also known as the wet phase; Chang *et al.*, 2016, figs 6–13), whereby the low-level northeasterly winds associated with a CS overwrite low-level southwesterly winds associated with the MJO wet phase when both are present.

When CS days coincide with the active anticyclonic vorticity phase (Figure 3b) located in the 100°–105°E band, the anomalous rainfall and low-level winds resemble the CS composite mean. This indicates that typical CSs occur with the anticyclonic vorticity phase located in this band. During the presence of the anticyclonic vorticity in the region on a CS day, a clear "parallel dipole pattern" between the Borneo coast and Indochina coast is observed with a "tick-mark-like" pattern of positive rainfall anomalies located in the SCS region. In northeastern Peninsular Malaysia, wet anomalies are replaced with dry anomalies as the wave progress to the west, a stark contrast to the enhanced rainfall anomalies during the CS days with the active cyclonic vorticity phase. One striking contrast between the anticyclonic vorticity phase and cyclonic vorticity phase on CS days is the anomalous northeasterly winds in the SCS. The northeasterly wind in the anticyclonic vorticity phase possesses a more northerly component and is stronger than the more zonally and weaker northeasterly wind during the cyclonic vorticity phase.

To investigate the difference between the vorticity phase of the wave on CS days, the difference in the low-level winds and rainfall between the anticyclonic and cyclonic phases (anticyclonic minus cyclonic vorticity; Figure 4) is plotted. The difference field shows clockwise circulation in the SCS and a counterclockwise circulation in the Philippines region. As the wave propagates westward from 110° to 115°E, the southeasterly flows in Peninsular Malaysia are replaced gradually by the northeasterly and easterly flows. The arrangement of the R1 wave is such that the anticyclonic vorticity phase is to the west while the cyclonic vorticity phase is to the east of the CS jet axis. This arrangement allows the jet-like wind in between the contrasting vorticity centres. The difference in the low-level winds shows that CS in the SCS is stronger (weaker) when the R1 wave located in the region is in the anticyclonic (cyclonic) phase. In this plot, the wind–terrain-induced rainfall and the rain parallel to the coast of western Borneo have been removed and dry (wet) anomalies are found in the vicinity of the anticyclonic (cyclonic) vorticity phase of the wave. This suggests that there is very little difference in the rainfall on the Borneo coast and that the impact of the vorticity phases on the CS rainfall is mainly in Peninsular Malaysia. Along the Equator, wet (dry) anomalies are found in the region of easterly (westerly) winds, suggesting the role of surface fluxes in the organization of convection.

4.2 | Extreme rainfall

In general, the CS events are known to increase the wet days frequency by more than 30% with respect to the seasonal wet days (days with rainfall ≥1 mm·day^{-1}) frequency (Figure 5a) in the region where the CS rainfall dominates. In the region of wet and dry anomalies parallel dipole, the rain intensity increases by at least 4 mm·day^{-1} with respect to the seasonal rain intensity in the wet anomaly region and decreases by at least 4 mm·day^{-1} with respect to the seasonal rain intensity (Figure 5b). The CS events also raise the likelihood of extreme rainfall events (rainfall exceeding the 95th percentile of precipitation of all days in the season during the period 1998–2018) as shown in Figure 5c. In the equatorial SCS and Java Sea where the CS rainfall dominates, extreme frequency increases by at least 10–20%.

When the CS events are stratified according to the active R1 vorticity phases, the rain and winds outline similarities and differences between these phases. The rainfall anomalies located in the vicinity of the active wave follow the sign of vorticity in the Northern Hemisphere. In regions where wind–terrain-induced rain dominates, the rainfall anomalies are generally the same regardless of the phase of the vorticity in the domain. However, in the locality where the wave is active, the rainfall anomaly alters. This is shown in Figure 3, where the rainfall anomaly pattern changes from a "tick-mark-like" pattern to a "V shape" when the local active anticyclonic domination is replaced by cyclonic vorticity domination in Peninsular Malaysia. Therefore, it is obvious that the phase of wave vorticity on CS days plays an important role in the distribution of regional rainfall. The impact of the CS days in different vorticity phases on the regional rainfall distribution is further investigated.

Figure 6 shows that large changes in wet days frequency with respect to seasonal wet days frequency are observed in the CS rainfall region (refer to Figure 1a). There is clearly a difference between the CS in the active cyclonic and anticyclonic vorticity phases, with the increased probabilities in the anticyclonic phase occurring over the southern part of the wave in the easterlies and the cyclonic phase tending to be more coincident with the centre of the vorticity. The magnitude of the changes is larger in the active cyclonic vorticity phase and in the oceanic region in both phases. In the active cyclonic vorticity phase, wet days frequency increases by at least more than 30–100% around the centre of vorticity. During the active anticyclonic vorticity phase, the wet days frequency increases by around 30–40% in the southern part of the wave. To the north of the anticyclonic centre, the likelihood of wet days decreases, and this contributes to the distinct north–south rainfall dipole, as seen in the rainfall composite. Contrarily, the large changes in the wet days during the cyclonic vorticity phase blurred the north–south rainfall dipole.

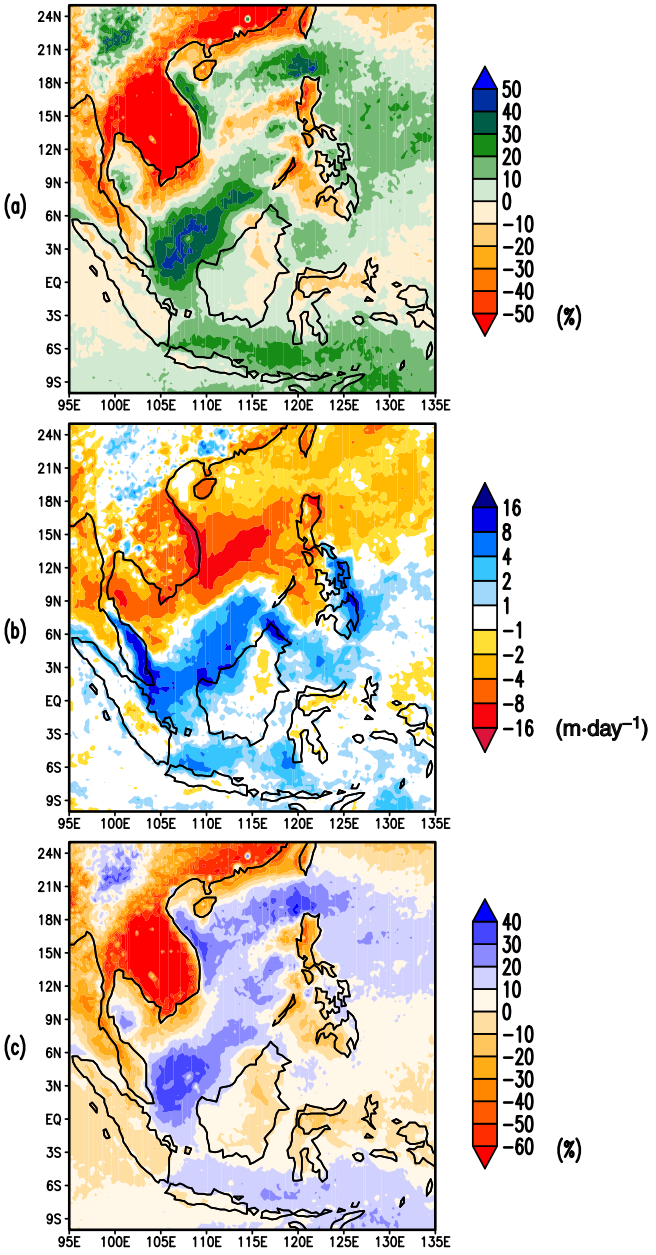

FIGURE 5 Composite difference between (a) cold surge (CS) wet days frequency and seasonal wet days frequency; (b) CS wet days intensity and seasonal wet days intensity; (c) CS extreme rainfall event frequency and seasonal extreme rainfall event frequency. Wet days are defined as days with rainfall ≥1 mm. Extreme rainfall events are defined as days with rainfall exceeding the 95th percentile of seasonal rainfall. The percentage is the percentage difference between CS wet days frequency and seasonal wet day frequency [Colour figure can be viewed at wileyonlinelibrary.com]

Along with the changes in the wet days frequency, the intensity of rainfall also changes. Figure 7 shows the changes in wet days intensity during a CS with active

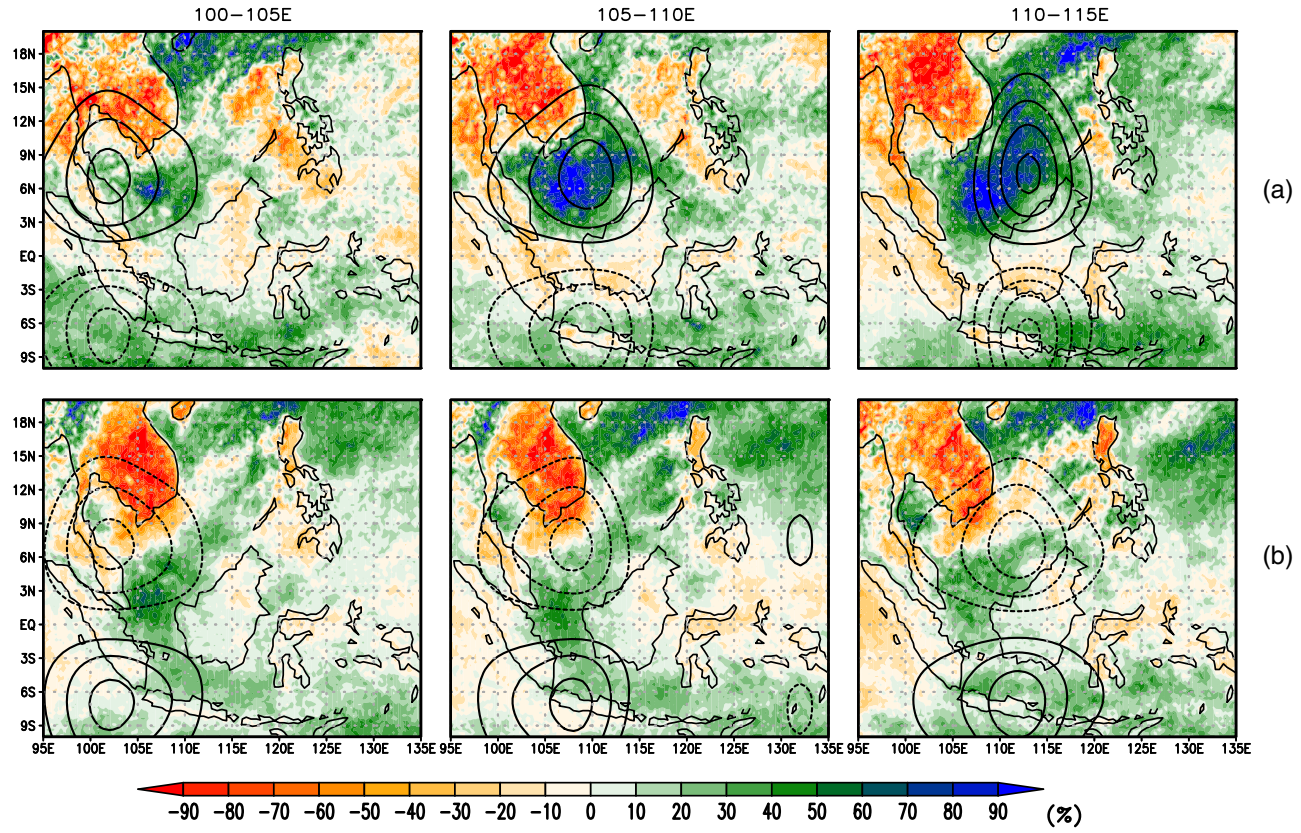

FIGURE 6 Composite of wet days frequency (shaded) percentage difference with respect to seasonal wet days frequency during cold surge (CS) active equatorial Rossby waves in the different longitudinal bands (contour): (a) cyclonic wave; (b) anticyclonic wave. The percentage is the percentage difference between CS wet days frequency and seasonal wet day frequency [Colour figure can be viewed at wileyonlinelibrary.com]

R1 wave days relative to the seasonal wet days intensity. In the anticyclonic phase, along the northeast–southwest tilt rainfall dipole (as shown in Figure 3b) there is a large change in the rainfall intensity. The rainfall intensity increases at least 4 mm·day^{-1} along the rainfall band that runs parallel to the Borneo coast and decreases at least 4 mm·day^{-1} in the Indochina region. As the vorticity centre traverses the SCS, the anomalous positive intensity on the northeast coast of Peninsular Malaysia weakens considerably, but there are only smaller changes in the intensity along the Borneo coast. During the CS days with active cyclonic phase in 110°–115°E, the intensity of the rainfall along the Borneo coast extends into the SCS, whereas downstream, on the northeast coast of Peninsular Malaysia, the intensity increase is not as large as the intensity increase during the anticyclonic phase in the same longitudinal band. This suggests that terrain-induced rainfall is modified by the large-scale wave dynamics where this would be coincident with the anticyclonic phase of the wave. As the wave propagates into the 100°–110°E bands, the intensity over the whole of the east coast of Peninsular Malaysia increases while the area of large intensity over the SCS shrinks and is confined nearer to the coast.

In the CS days with cyclonic vorticity phase, extreme rainfall frequency increases by at least 40% around the vicinity of the vorticity, whereas in the anticyclonic vorticity phase the extreme frequency decreases around 20% and has a smaller area coverage (Figure 8). The large increase in the extreme frequency in the Indochina region can be attributed to the fact that the region is dry during this time of the year and even a small increase in the amount of rainfall can contribute to an amount exceeding the 95th percentile in the region. In Peninsular Malaysia, the signal of the extreme frequency changes gradually from negative anomalies to positive anomalies as the active cyclonic vorticity propagates from 110°–115°E to 100°–105°E. However, when the active anticyclonic vorticity propagates from 110°–115°E to 100°–105°E, the extreme rainfall frequency increase in Peninsular Malaysia remains relatively unchanged around 0–20% except for a small decrease on the northeast coast of Peninsular Malaysia (to around 0–10%).

To summarize, the changes in frequency for wet days and extreme events are larger in the cyclonic vorticity, whereas the rainfall intensity changes are almost equal in the two vorticity phases. One of the largest differences

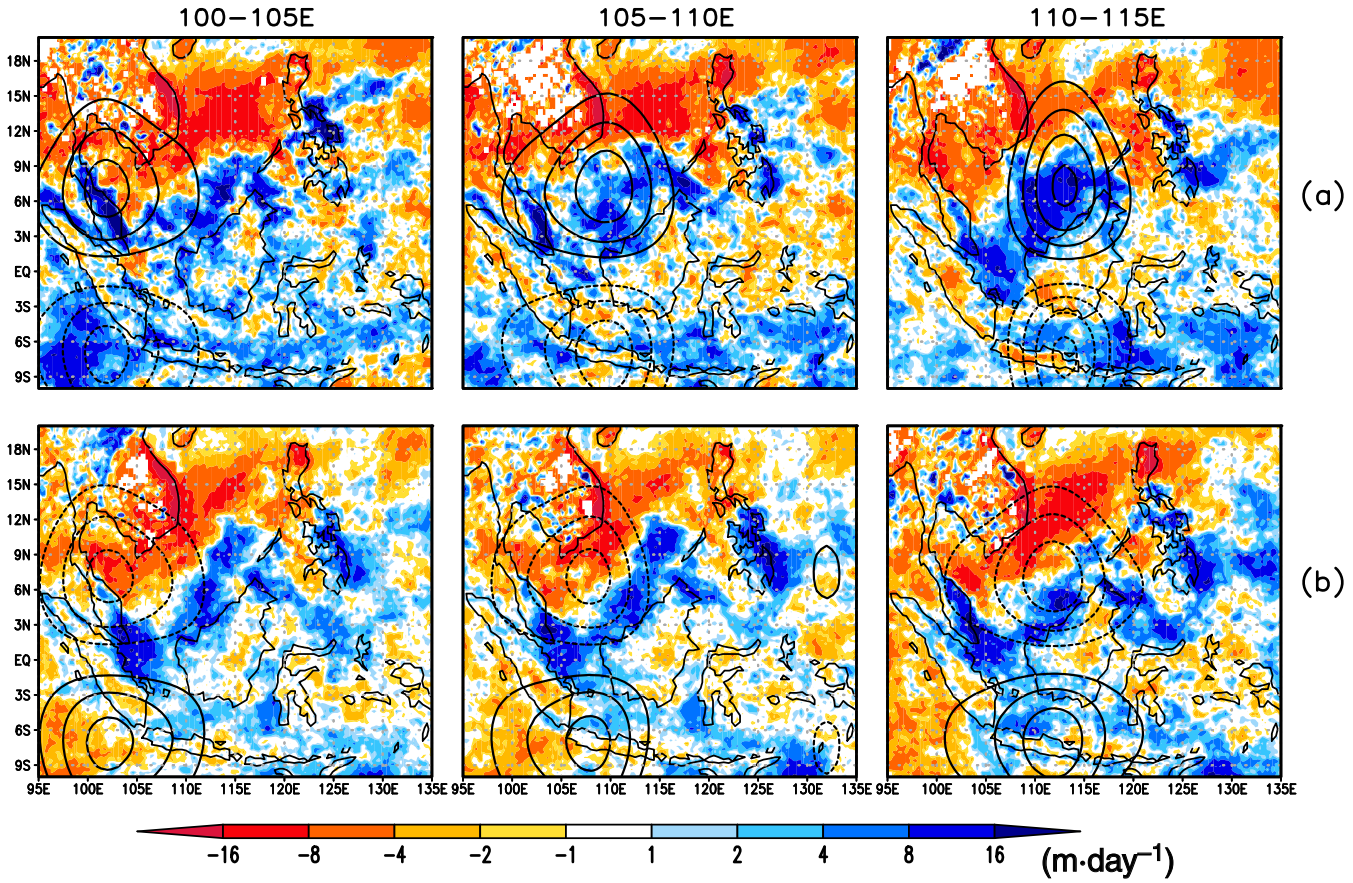

FIGURE 7 Composite of wet days intensity difference (shaded) with respect to seasonal wet days intensity during cold surge active equatorial Rossby waves in the different longitudinal bands (contour): (a) cyclonic wave; (b) anticyclonic wave [Colour figure can be viewed at wileyonlinelibrary.com]

between the cyclonic and anticyclonic phases is the large increases in the intensity and frequency are confined mainly nearer to the Equator during the anticyclonic phase, whereas during the cyclonic phase the increase covers a wider region. The similarity between the intensity changes features and the precipitation composite suggests that the precipitation anomalies are dominated by changes in intensity on wet days rather than the number of wet days.

4.3 | Evolution of the CSs and their relation with the vorticity phase of R1

In Table 1 and Section 4.1, we have shown the existence of active R1 waves with cyclonic vorticity on CS days. Since Lim and Chang (1981) showed that the mid-latitude anticyclone extended into the Equator in the northeast–southwest tilt due to the dispersion of various meridional Rossby waves. The existence of cyclonic vorticity on CS days is therefore worth investigating. As some CSs are known to be relatively drier than others, does the phase of R1 vorticity explain some basic differences between surge episodes? To investigate the difference, we look into the evolution of the composite CS events in 105°–110°E since the majority of an active wave on CS days takes place in this longitude. The lead–lag anomaly composites are constructed from the CS dates with the same vorticity phase of active R1 waves by removing the NDJFM mean. To avoid resampling the same event being composite, the CS and active R1 wave dates that fall within a ±3 days period in the same vorticity sign are removed from the composite. By doing so we ensure that the events are defined only once. Figures 9 and 10 show lead–lag composites for vorticity (contour), wind anomaly (vector), and rainfall anomaly (shaded) for active R1 vorticity on CS days. The days are categorized as day −6, day −4, day −2, day 0, day +2, and day +4. Here, the minus (plus) sign represents the days preceding (following) the day when the CSs coincide with the active R1 wave (day 0).

Figure 9 shows the evolution of the composite CS coincides with the active R1 cyclonic phase on day 0 in 105–110 E. On day −6, R1 cyclonic vorticity is located in the Philippines region while R1 anticyclonic vorticity is

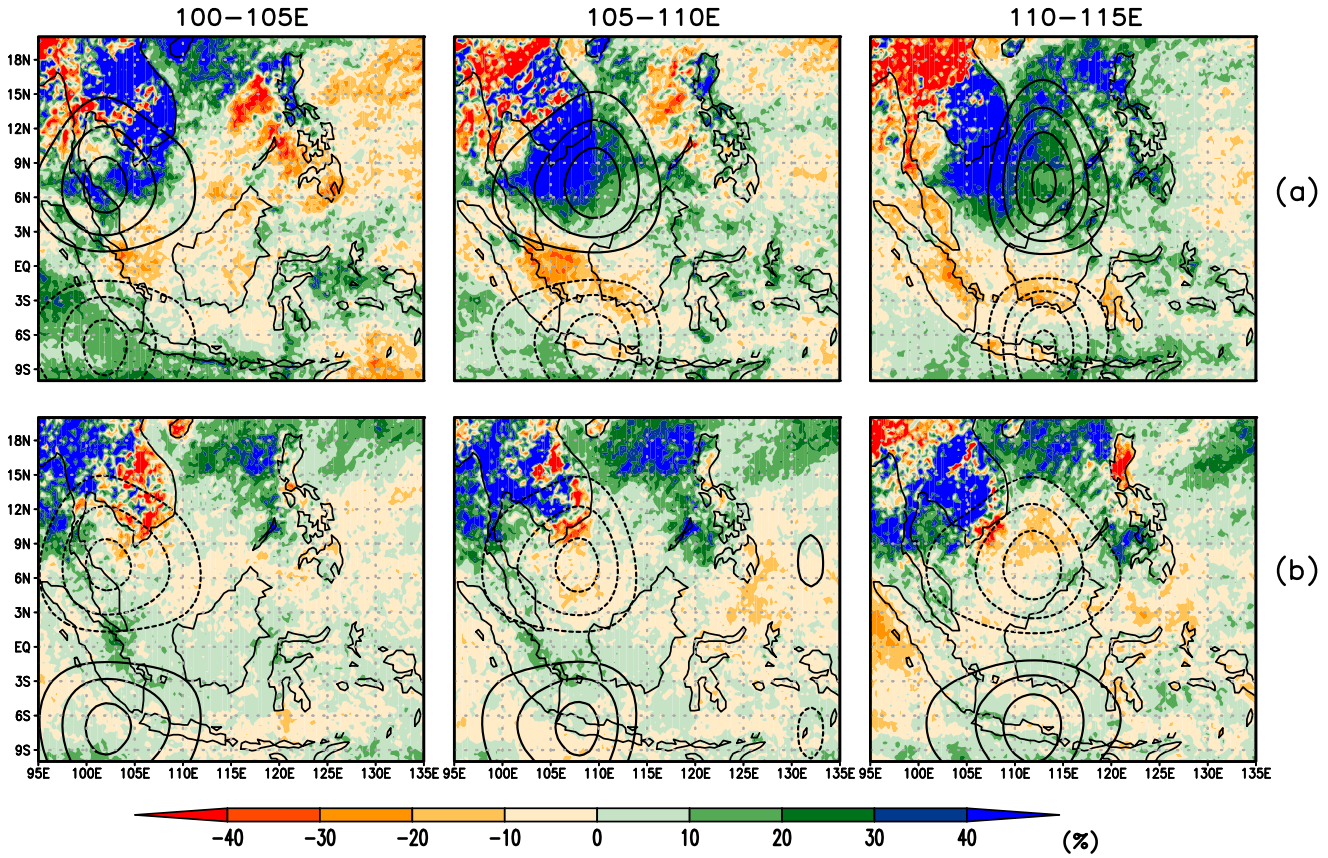

FIGURE 8 Composite of extreme rainfall event frequency difference (shaded) with respect to seasonal extreme rainfall event frequency during active equatorial Rossby waves in the different longitudinal bands (contour): (a) cyclonic wave; (b) anticyclonic wave [Colour figure can be viewed at wileyonlinelibrary.com]

located in the SCS–Malaysia region. In the SCS region, anomalous rainfall is observed along the coast of Borneo and the southeastern coast of Peninsular Malaysia. At the same time, rainfall is suppressed in the northeastern coast of Peninsular Malaysia. Winds in the SCS are predominantly anomalous northeasterly. By day −4, the anomalous northeasterly winds in the SCS strengthen considerably. With the presence of organized R1 anticyclonic vorticity in the SCS, the rain band along the coast of Borneo weakens. On day −2, the R1 cyclonic vorticity originally located in the Philippines now propagates westward and strengthens. The rainfall around this cyclonic vorticity becomes organized and spread along the Borneo coast. To the north of this rain band, the rainfall is suppressed. This forms the wet and dry anomalies northeast–southwest tilt "parallel dipole" mentioned in Section 3. During this time, the winds in the SCS are anomalously strong northeasterly originating from the east Asia continent. This indicates the CS is observed on day −2. The R1 anticyclonic and cyclonic vorticities are located respectively to the west and east of the CS axis. On day 0, the R1 cyclonic vorticity is now located in 105°–110°E and the anticyclonic vorticity has propagated further westward and is no longer seen here. Correspondingly, the rain band also propagates westward. As a result, the regionwide suppressed rainfall in Peninsular Malaysia observed on day −2 is replaced by enhanced rain, especially over its east coast region. The CS northeasterly winds now become increasingly zonal. This suggests that the northeast–southwest tilt of the CS axis becomes more zonal. On day +2, the SCS and regions surrounding it are now dominated by a broad easterly. Enhanced rainfall is now observed in the Peninsular Malaysia region due to the R1 cyclonic vorticity. The "parallel dipole pattern" becomes obscure on day +0 when the R1 cyclonic vorticity propagates into the centre of southern SCS replacing the R1 anticyclonic vorticity. The anomalous dry weather in Peninsular Malaysia seen on day −2 with R1 anticyclonic is replaced by anomalous wet weather on day +2 with R1 cyclonic vorticity.

Figure 10 shows the evolution of the composite CS coincides with the active R1 anticyclonic phase on day 0 in 105°–110 E. The CS is observed on day 0 in this vorticity phase with R1 anticyclonic vorticity to the west and R1 cyclonic vorticity to the east of the CS axis. In the SCS region, the winds are predominantly northnortheasterly. The anomalous rainfall shows a "V-shape" pattern during

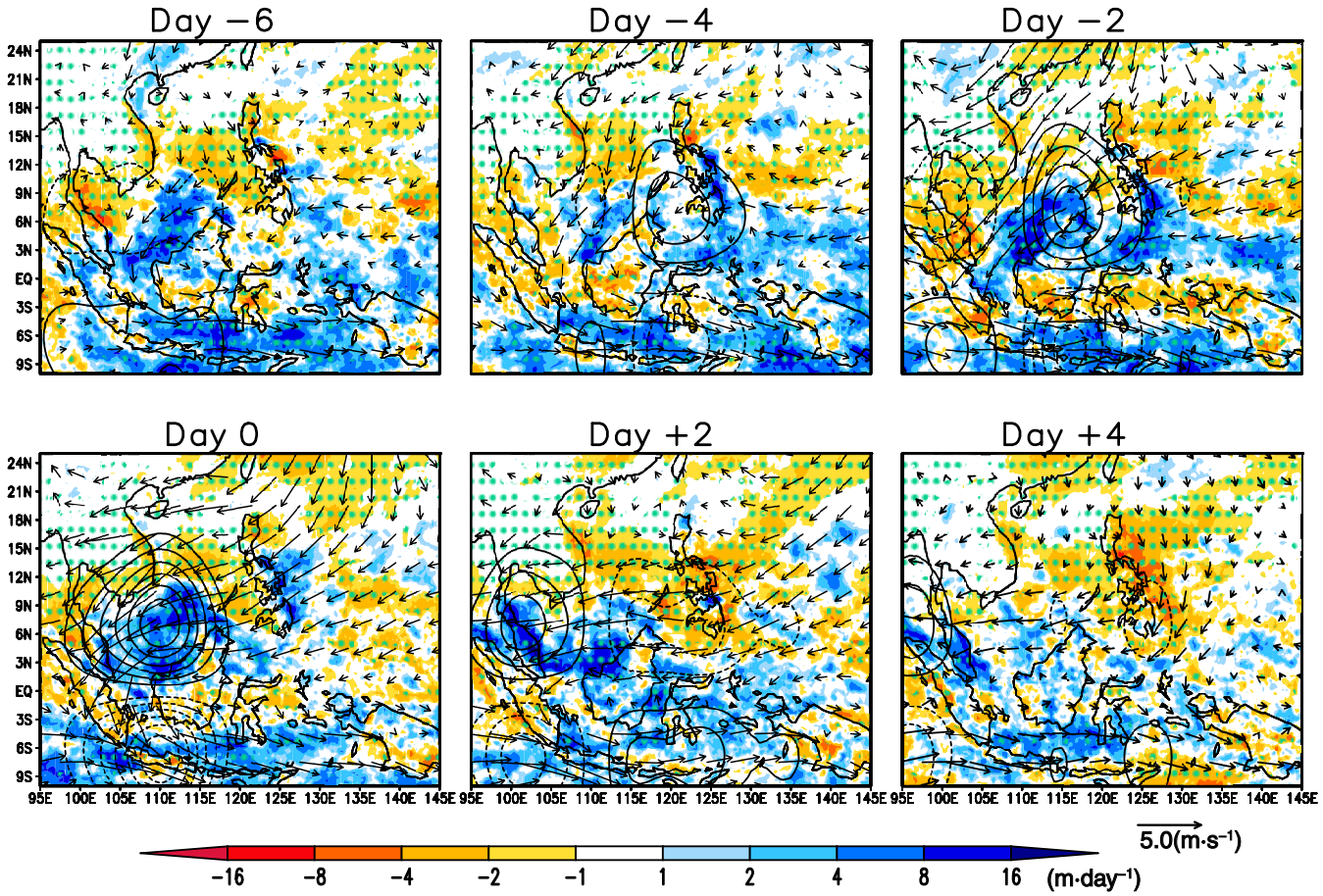

FIGURE 9 Evolution of cold surge (CS) events for active cyclonic vorticity in 105°–110°E from day −8 to day +5. Day 0 indicates active wave day in the selected longitude on CS days. Vorticity contours start $\pm 5 \times 10^{-6}$ s^{-1} with an interval of 5×10^{-6} s^{-1}. Shaded: precipitation anomaly; contour: vorticity; and vector: wind anomaly. Anomalies are calculated by removing the seasonal mean. Stippling indicates regions where anomaly is significantly different from the 20 November–March seasonal mean at the 95% confidence level based on Student's *t*-test [Colour figure can be viewed at wileyonlinelibrary.com]

this time with suppressed rainfall observed slightly to the north of R1 anticyclonic vorticity in the centre of the southern SCS. In the same region, the rainfall "parallel dipole pattern" begins to emerge. As the R1 anticyclonic vorticity propagates into the Peninsular Malaysia region on day +2, its northern region experiences anomalous dry weather. This resulted in the "parallel dipole pattern" becoming more distinct. The northnortheasterly winds in the region become eastnortheasterly. From day 0 to day +2, the CS axis tilt increases.

From Figures 9 and 10, during the early stage of a CS, the arrangement of the R1 vorticity is anticyclonic located to the west and cyclonic located to the east of the CS axis. This shows R1 anticyclonic vorticity is always located to the west of the CS axis in the initial stage of the CS. This arrangement allows jet-like wind in between the contrasting vorticity centre. Therefore, this is consistent with the theory of Lim and Chang (1981) that showed the CS is indeed the midlatitude anticyclone extended into the Equator. The dispersion of various Rossby Hermite modes that contribute to the northeast–southwest tilt of the midlatitude anticyclone as stated by Lim and Chang (1981) can also be seen in the CS axis in Figures 9 and 10. This dispersion of the Rossby Hermite modes argument is further supported by the evidence that the CS axis becomes more zonal in the later part of the CS. Since the R1 mode is the gravest mode and is located in the equatorial region, the R1 mode therefore makes up the southwest end of the CS axis. The R1 also propagates westward faster than the higher modes in midlatitudes. As the southwest end of the axis (R1 anticyclonic vorticity) propagates faster westward (for cyclonic case, from day −2 to day 0; for anticyclonic case, from day 0 to day +2), the axis becomes more zonal. However, from the analysis of the composite, we also notice that the midlatitude anticyclone propagates slightly eastward after the initial CS, which is not discussed by Lim and Chang (1981). This also contributes to the CS axis tilt becoming zonal.

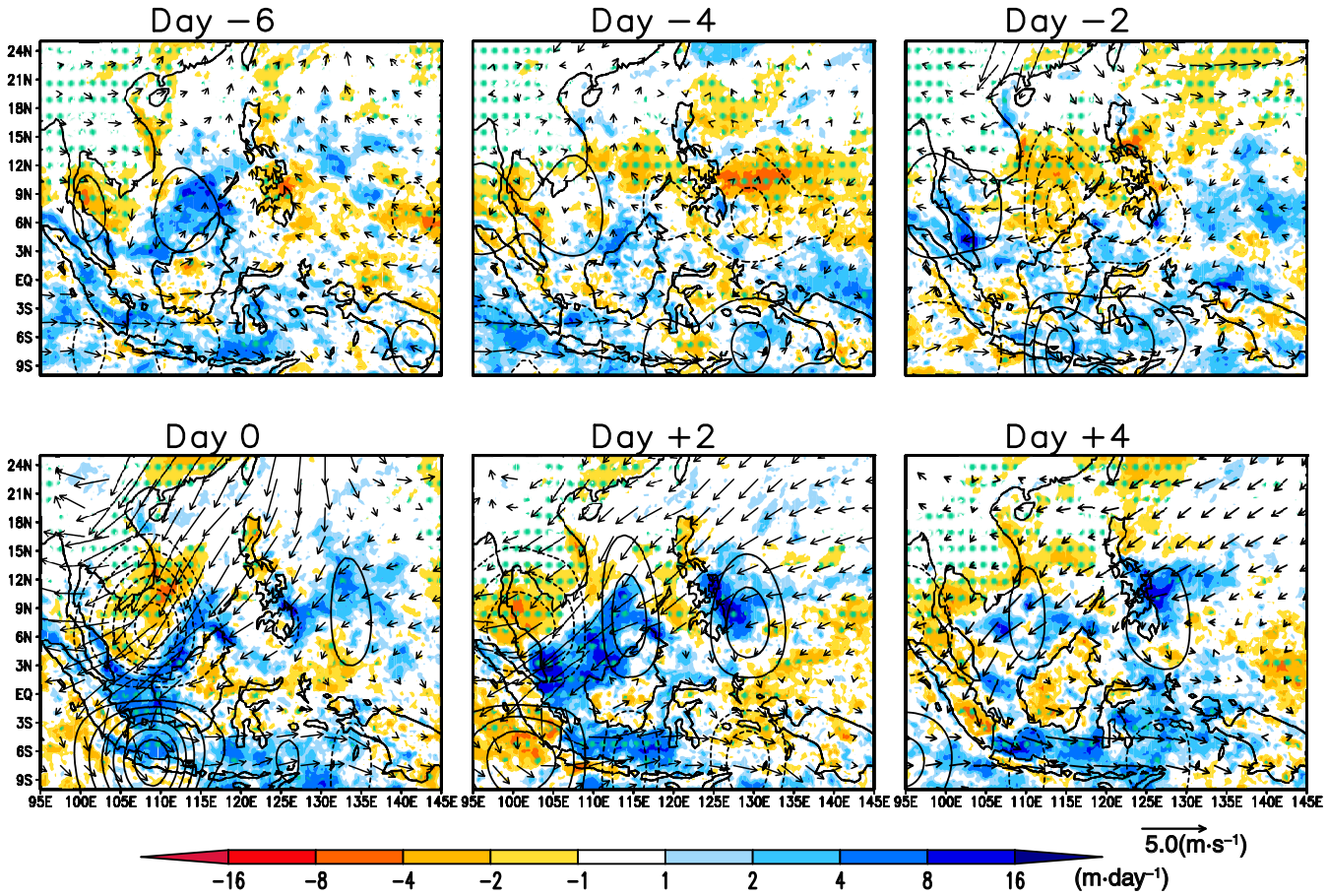

FIGURE 10 As Figure 9 but for anticyclonic vorticity [Colour figure can be viewed at wileyonlinelibrary.com]

The CS events are accompanied by enhanced rain in the SCS–MC region. Although, in general, rainfall is found on the windward side of the terrain and along the coast of Borneo during a CS, the rainfall distribution in the region for the two vorticity phases is different. For instance, during the early stage of a CS in the cyclonic phase case (day −2, Figure 9) Peninsular Malaysia is anomalously dry, whereas in the anticyclonic phase case (day 0, Figure 10) Peninsular Malaysia is anomalously wet. It is also clear from the analysis that the anomalous wet (dry) weather in the region can be replaced with the anomalous dry (wet) weather when the R1 anticyclonic (cyclonic) vorticity propagates into the region. In short, the rainfall pattern in the region changes along with the propagation of the R1 wave. This shows the large-scale R1 wave dynamics do, to some extent, modify the rain distribution on CS days. To show this, the time composite rainfall from two principal stations obtained from the Malaysian Meteorological Department are analysed. Figure 11 shows during the active cyclonic phase in 105°–110°E, rain recorded in Kuching Station (located to the east of the wave; Figure 11b) peaks between day −3 and day −1 and reduces significantly afterwards. A contrasting pattern in the local rain pattern is observed in the Kota Bahru station (Figure 11a), which is located to the west of the wave. Similar patterns are also observed for the extreme rain events represented by the 99th percentile in the respective stations. To show the consistency of this rain evolution, the difference between the 5-day mean rainfall before day 0 and the 5-day mean rainfall after day 0 are calculated for 66 CSs coincide with anticyclonic events and 38 CSs coincide with cyclonic events. A negative (positive) difference indicates a decrease (increase) in the rainfall after day 0. In the anticyclonic events, out of 66 rainfall events recorded in Kota Bharu and Kuching, about 66% (55%) of them show a decrease (increase) in the 5-day mean rainfall after day 0 in Kota Bharu (Kuching). The difference also indicates that about 64% (61%) of the 38 rainfall events recorded in Kota Bharu (Kuching) show an increment (reduction) in the rainfall during cyclonic events. This shows that maximum rain shifted from east to west for about 3–5 days during the CS in the active cyclonic phase. The opposite happens during the CS in the active anticyclonic phase. A caveat here is the use of the R1 only to explain the large-scale dynamics although some other equatorial waves may also play a role in explaining the large-scale rain.

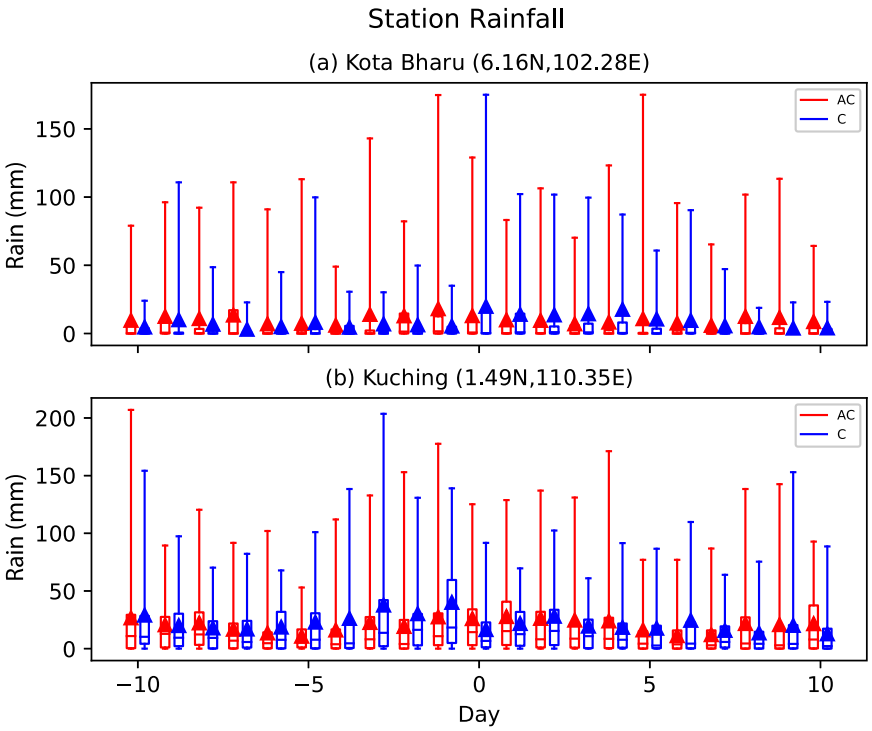

FIGURE 11 A box-and-whiskers plot of daily rainfall in (a) Kota Bharu station (6.16°N, 102.28°E) and (b) Kuching station (1.49°N, 110.35°E) when cold surge days coincide with active $n = 1$ Rossby wave located in 105°–110°E on day 0 as a function of days preceding and after. Boxes represent rainfall within the first and third quartiles. The line represents the median, and the triangle represents the mean. The bottom and top edges of the whisker represent the 1st and 99th percentiles. [Colour figure can be viewed at wileyonlinelibrary.com]

5 | CONCLUDING REMARKS

A large fraction of rainfall variability during the winter monsoon in the southeast Asia MC is contributed by the northeasterly CSs. The rainfall associated with the CSs is concentrated mainly over the windward side of the islands and peninsula, which represents strong influences of the local terrain. Tropical waves are known to play an important role in modulating tropical weather on a large scale. The study aims to understand the process that determines the regional rainfall distribution during CS days by looking at the different vorticity phases of active ER waves in three different longitude bands and also to verify the findings of Lim and Chang (1981) by using the R1 waves derived from ERA-INT.

On the CS days' composite mean, the R1 wave organized itself with anticyclonic and cyclonic vorticity located respectively to the west and east of the downstream CS. This suggests consistency with the theory of Lim and Chang (1981), in which the anticyclonic outflow originating from the midlatitude forcing behaves like a dispersive group of ER meridional modes that are manifested by the northeast–southwest tilt of the jet-like winds belt. Statistics showed that, on the CS days, the anticyclonic vorticity phases account for more than 50% of the total CS days. As the anticyclonic vorticity identified is located closer to Peninsular Malaysia, the number of anticyclonic vorticity phases accounts for over more than 60% of the total CS days. Likewise, the result also shows the number of CS days with the active anticyclonic phase is more than the CS days with the cyclonic phase. Thus, this suggests the region to the west of 110°–115°E is the preferred CS axis. If the CSs are thought to be the ER wave dispersive group in anticyclonic vorticity phases, then how would the rest of the total CS days (almost 40%) be associated with the cyclonic vorticity? The time evolution of composite CSs from day −6 to day +4 shows that the active cyclonic vorticity phase in the selected longitudes is due to the westward propagation of the R1 wave. In this case, the CSs start 3 days earlier, before the active cyclonic vorticity phase propagates into or intensifies in the identified longitudes, and are no longer seen by day +2. However, in the active vorticity phase, the CS starts on day 0 and lasted no longer than day +4. This shows that the CS events are longer in the active cyclonic vorticity phase. In both cases, the anticyclonic vorticity phase is located to the west of the CS axis. This is in agreement with the findings of Lim and Chang (1981) and reaffirms that the CSs are indeed the midlatitude anticyclones that extend into the Equator. The results also show that the northeasterly winds become more zonal in both cases. The changing of the winds indicates the changing in the tilt of the CS axis and indirectly show that the CSs' northeast–southwest tilt is the result of the Rossby meridional dispersion. Since the R1 wave is the gravest mode and located in the equatorial region, it makes up the southwest end of the CS axis. Since in the cyclonic case the CS lasted longer, the R1 anticyclonic vorticity would have propagated much further westward. On that account, this contributes to the tilting of the CS axis or the winds becoming more zonal compared with the anticyclonic case.

Heavy rainfall in the region during the winter monsoon in the region is normally caused by CSs. Since the CSs' impact on the rainfall is primarily driven by wind–terrain interaction and ER wave is part of the CSs, it is natural to show the impact of regional rainfall distribution when CSs coincide with an active wave. This reveals that in all the vorticity phases the region immediately to the west of the CS axis is drier during the initial stage of the CSs due to the presence of the R1 anticyclonic vorticity phase in this region. However, when the active cyclonic vorticity phase propagates into the region, the rainfall is enhanced. There is also evidence from the observation that the R1 vorticity phase modifies the local rain when the associated large-scale organized enhanced/suppressed rain propagates into the region. Therefore, this provides information on the possible enhancement or suppression of rainfall along with the westward movement of the active vorticity phase during CSs. When the active cyclonic phase is located in the central equatorial SCS, the north–south parallel wet–dry dipole becomes obscure due to the larger spatial extent of rain in the southern pole. As the active cyclonic vorticity phase propagates into Peninsular Malaysia, the rainfall "tick-mark-like" pattern in the region becomes a "V-shape" pattern. The similarity in the rainfall distribution between co-occurrence of the CS–MJO wet phase and the active cyclonic phase on the CS may indicate interaction between the R1 wave forced by the midlatitude and those from the MJO envelope. However, this is beyond the scope of the present study. This study also shows that the changes in the probability of wet days and frequency of extreme events are larger in the cyclonic vorticity phase but are almost equal for the intensity changes between the two vorticity phases. Furthermore, the similarity between the intensity changes features and the rainfall composite suggested that the rainfall anomalies are dominated by the changes of intensity on wet days. In addition, during the CSs, on the northeast coast of Peninsular Malaysia, the intensity increases (decreases) as the active cyclonic (anticyclonic) phase propagates toward the peninsula. These changes indicate the role of the active R1 wave in the rainfall distribution on CS days. This, together with the timing of the enhancement or suppression of rain, will provide additional valuable information to help improve predictions of extreme weather events.

AUTHOR CONTRIBUTIONS

Jeong-Yik Diong: Conceptualization; data curation; formal analysis; methodology; software; visualization; writing – original draft. **Prince Xavier:** Conceptualization; methodology; project administration; writing – review and editing. **Steve Woolnough:** Conceptualization; methodology; writing – review and editing. **Firdaus Ammar Abdullah:** Conceptualization; funding acquisition; project administration; writing – review and editing.

ACKNOWLEDGEMENTS

This work and its contributors were supported by the Weather and Climate Science for Services Partnership (WCSSP) Southeast Asia. The first and last authors would like to thank the Director-General of the Malaysian Meteorological Department for supporting this work. The first author would also like to thank the National Centre for Atmospheric Science (NCAS), University of Reading, for hosting his visit during the preliminary stage of this work. Prince Xavier was supported by the Met Office Weather and Science for Services Partnership (WCSSP) Southeast Asia as part of the Newton Fund. Steven J. Woolnough was also supported by the NCAS ODA national capability program ACREW (NE/R000034/1), which is supported by NERC and the GCRF.

ORCID

Jeong-Yik Diong https://orcid.org/0000-0003-1128-7425

REFERENCES

Chang, C.-P., Erikson, J. and Lau, K. (1979) Northeasterly cold surges and near-equatorial disturbances over the winter MONEX area during December 1974. Part I L synoptic aspects. *Monthly Weather Review*, 107, 812–829.

Chang, C.P., Harr, P.A. and Chen, H.J. (2005a) Synoptic disturbances over the equatorial South China Sea and western maritime continent during boreal winter. *Monthly Weather Review*, 133, 489–503. https://doi.org/10.1175/MWR-2868.1.

Chang, C.P., Liu, C.H. and Kuo, H.C. (2003) Typhoon Vamei: an equatorial tropical cyclone formation. *Geophysical Research Letters*, 30, 10–13. https://doi.org/10.1029/2002GL016365.

Chang, C.-P., Lu, M.-M. and Lim, H. (2016) Monsoon convection in the maritime continent: interaction of large-scale motion and complex terrain. *Meteorological Monographs*, 56, 6.1–6.29. https://doi.org/10.1175/amsmonographs-d-15-0011.1.

Chang, C.P., Wang, Z. and Hendon, H. (2006) The Asian winter monsoon. In: Wang, B. (Ed.) *The Asian Monsoon*. Berlin: Praxis, pp. 89–127.

Chang, C.P., Zhuo, W., John, M. and Ching-Hwang, L. (2005b) Annual cycle of Southeast Asia—maritime continent rainfall and the asymmetric. *Journal of Climate*, 18, 287–301.

Cheang, B.K. (1977) Synoptic features and structures of some equatorial vortices over the South China Sea in the Malaysian region during the winter monsoon, December 1973. *Pure and Applied Geophysics*, 115, 1303–1333.

Chen, T.C., Tsay, J.D., Yen, M.C. and Matsumoto, J. (2013) The winter rainfall of Malaysia. *Journal of Climate*, 26, 936–958. https://doi.org/10.1175/JCLI-D-12-00174.1.

Chen, W.T., Hsu, S.P., Tsai, Y.H. and Sui, C.H. (2019) The influences of convectively coupled Kelvin waves on multiscale rainfall variability over the South China Sea and maritime continent in

December 2016. *Journal of Climate*, 32, 6977–6993. https://doi.org/10.1175/JCLI-D-18-0471.1.

Dee, D.P., Uppala, S.M., Simmons, A.J., Berrisford, P., Poli, P., Kobayashi, S., Andrae, U., Balmaseda, M.A., Balsamo, G., Bauer, P., Bechtold, P., Beljaars, A.C.M., van de Berg, L., Bidlot, J., Bormann, N., Delsol, C., Dragani, R., Fuentes, M., Geer, A.J., Haimberger, L., Healy, S.B., Hersbach, H., Hólm, E.V., Isaksen, L., Kållberg, P., Köhler, M., Matricardi, M., McNally, A.P., Monge-Sanz, B.M., Morcrette, J.-J., Park, B.-K., Peubey, C., de Rosnay, P., Tavolato, C., Thépaut, J.-N., Vitart, F. (2011) The Era Interim reanalysis: configuration and performance of the data assimilation system. *Quarterly Journal of the Royal Meteorological Society*, 137, 53–597. https://doi.org/10.1002/qj.828

Ferrett, S., Yang, G.Y., Woolnough, S.J., Methven, J., Hodges, K. and Holloway, C.E. (2020) Linking extreme precipitation in Southeast Asia to equatorial waves. *Quarterly Journal of the Royal Meteorological Society*, 146, 665–684. https://doi.org/10.1002/qj.3699.

Hai, O.S., Samah, A.A., Chenoli, S.N., Subramaniam, K. and Mazuki, M.Y.A. (2017) Extreme rainstorms that caused devastating flooding across the east coast of peninsular Malaysia during November and December 2014. *Weather and Forecasting*, 32, 849–872. https://doi.org/10.1175/WAF-D-16-0160.1.

Huffman, G.J., Adler, R.F., Bolvin, D.T., Gu, G., Nelkin, E.J., Bowman, K.P., Hong, Y., Stocker, E.F., Wolff, D.B. (2007) The TRMM multi-satellite precipitation analysis: Quasi-global, multi-year, combined-sensor precipitation estimates at fine scale. *Journal of Hydrometeorology*. 8, 38–55. https://doi.org/10.1175/JHM560.1.

Johnson, R.H. and Chang, C.P. (2007) Winter MONEX-a quarter-century and beyond. *Bulletin of the American Meteorological Society*, 88, 385–392. https://doi.org/10.1175/bams-88-3-385.

Johnson, R.H. and Houze, R.A. (1987) Precipitating cloud systems of the Asian monsoon. In: Chang, C.P. and Krishnamurti, T. (Eds.) *Monsoon Meteorology*. Oxford: Oxford University Press, pp. 298–353.

Kiladis, G.N., Wheeler, M.C., Haertel, P.T., Straub, K.H. and Roundy, P.E. (2009) Convectively coupled equatorial waves. *Reviews of Geophysics*, 47, 1–42. https://doi.org/10.1029/2008RG000266.

Latos, B., Lefort, T., Flatau, M.K., Flatau, P.J., Permana, D.S., Baranowski, D.B., Paski, J.A., Makmur, E., Sulystyo, E., Peyrillé, P. and Feng, Z. (2021) Equatorial waves triggering extreme rainfall and floods in Southwest Sulawesi. *Indonesia Monthly Weather Review*, 149, 1381–1401. https://doi.org/10.1175/MWR-D-20-0262.1.

Liebmann, B. and Hendon, H.H. (1990) Synoptic-scale disturbances near the equator. *Journal of the Atmospheric Sciences*, 47, 1463–1479.

Lim, H. and Chang, C.P. (1981) A theory for Midlatitude forcing of tropical motions during winter monsoon. *Journal of the Atmospheric Sciences*, 38, 2377–2392.

Lim, S.Y., Marzin, C., Xavier, P., Chang, C.P. and Timbal, B. (2017) Impacts of boreal winter monsoon cold surges and the interaction with MJO on Southeast Asia rainfall. *Journal of Climate*, 30, 4267–4281. https://doi.org/10.1175/JCLI-D-16-0546.1.

Lubis, S.W. and Respati, M.R. (2021) Impacts of convectively coupled equatorial waves on rainfall extremes in Java. *International Journal of Climatology*, 41, 2418–2440. https://doi.org/10.1002/joc.6967.

Pullen, J., Gordon, A.L., Flatau, M., Doyle, J.D., Villanoy, C. and Cabrera, O. (2015) Journal of geophysical research: atmospheres rainfall in The Philippines. *Journal of Geophysical Research–Atmospheres*, 120, 3292–3309. https://doi.org/10.1002/2014JD022645.Received.

Ramage, C.S. (1971) *Monsoon Meteorology*. London: Academic Press, p. 300.

Roundy, P.E. and Frank, W.M. (2004) A climatology of waves in the equatorial region. *Journal of the Atmospheric Sciences*, 61, 2105–2132. https://doi.org/10.1175/1520-0469(2004)061<2105:ACOWIT>2.0.CO;2.

Tangang, F.T., Juneng, L., Salimun, E., Vinayachandran, P.N., Seng, Y.K., Reason, C.J.C., Behera, S.K. and Yasunari, T. (2008) On the roles of the northeast cold surge, the Borneo vortex, the Madden-Julian Oscillation, and the Indian Ocean Dipole during the extreme 2006/2007 flood in southern peninsular Malaysia. *Geophysical Research Letters*, 35, 1–6. https://doi.org/10.1029/2008GL033429.

Tsai, W.Y.-H., Lu, M.-M., Sui, C.-H. and Lin, P.-H. (2020) MJO and CCEW modulation on South China Sea and maritime continent boreal winter subseasonal peak precipitation. *Terrestrial, Atmospheric and Oceanic Sciences*, 31, 177–195. https://doi.org/10.3319/tao.2019.10.28.01.

Wheeler, M. and Kiladis, G.N. (1999) Convectively coupled equatorial waves: analysis of clouds and temperature in the wavenumber-frequency domain. *Journal of the Atmospheric Sciences*, 56, 374–399. https://doi.org/10.1175/1520-0469(1999)056<0374:CCEWAO>2.0.CO;2.

Wheeler, M., Kiladis, G.N. and Webster, P.J. (2000) Large-scale dynamical fields associated with convectively coupled equatorial waves. *Journal of the Atmospheric Sciences*, 57, 613–640. https://doi.org/10.1175/1520-0469(2000)057<0613:LSDFAW>2.0.CO;2.

Wu, M. and Chan, J.C. (1995) Surface features of winter monsoon surges over South China. *Monthly Weather Review*, 123, 662–680.

Xavier, P., Lim, S.Y., Ammar Bin Abdullah, M.F., Bala, M., Chenoli, S.N., Handayani, A.S., Marzin, C., Permana, D., Tangang, F., Williams, K.D. and Yik, D.J. (2020) Seasonal dependence of cold surges and their interaction with the Madden–Julian Oscillation over Southeast Asia. *Journal of Climate*, 33, 2467–2482. https://doi.org/10.1175/JCLI-D-19-0048.1.

Yang, G.Y., Hoskins, B. and Slingo, J. (2003) Convectively coupled equatorial waves: a new methodology for identifying wave structures in observational data. *Journal of the Atmospheric Sciences*, 60, 1637–1654. https://doi.org/10.1175/1520-0469(2003)060<1637:CCEWAN>2.0.CO;2.

Yang, G.Y., Hoskins, B. and Slingo, J. (2007) Convectively coupled equatorial waves. Part I: horizontal and vertical structures. *Journal of the Atmospheric Sciences*, 64, 3406–3423. https://doi.org/10.1175/JAS4017.1.

How to cite this article: Diong, J.Y., Xavier, P., Woolnough, S.J. & Abdullah, F.A. (2023) Equatorial Rossby waves on cold surge days and their impact on rainfall. *Quarterly Journal of the Royal Meteorological Society*, 1–17. Available from: https://doi.org/10.1002/qj.4493